Supporting Information for

Unveiling the electrocatalytic potential of main-group metal-doped blue phosphorene for oxygen and hydrogen evolution reaction through computational study

Hao Hu,[a] Yang-Chun Yong,*[b] Peng Zhang,[c] Wei Tang,[a] Bei-Bei Xiao,[d] and Jian-Li Mi*[a]

[a] *Institute for Advanced Materials, School of Materials Science and Engineering, Jiangsu University, Zhenjiang 212013, China*

[b] *Biofuels Institute, School of Environment and Safety Engineering, Jiangsu University, Zhenjiang 212013, China*

[c] *Key Laboratory for Water Quality and Conservation of the Pearl River Delta, Ministry of Education, Institute of Environmental Research at Greater Bay, Guangzhou University, Guangzhou 510006, China*

[d] *School of Energy and Power Engineering, Jiangsu University of Science and Technology, Zhenjiang 212003, China*

Calculation methods

The Gibbs free energy diagrams of OER/HER are calculated using the reversible hydrogen electrode (RHE) model developed by Nørskov et al..[1] Taken RHE as the reference electrode, the chemical potential (μ) of proton-electron pair is equal to that of half a hydrogen molecule:

$$\mu_{H^+} + \mu_{e^-} = \frac{1}{2}\mu_{H_2} \quad (1)$$

at conditions with $U = 0$ V and $P_{H_2} = 1$ bar.

The free energies (G) of each species are calculated as:

$$G = E_{DFT} + E_{ZPE} - TS \quad (2)$$

where the E_{DFT} is the DFT calculated total energy, E_{ZPE} is zero-point energy and S is the entropy at 298 K. Since the exact free energy of OH, O, OOH and H radicals in the electrolyte solution is difficult to obtain, the adsorption free energy ΔG_{OH*}, ΔG_{O*}, ΔG_{OOH*} and ΔG_{H*} are relative to the free energy of stoichiometrically appropriate amounts of H_2O (l) and H_2 (g), defined as follows:

$$\Delta G_{OH*} = G_{OH*} - G_* - (G_{H_2O} - \frac{1}{2}G_{H_2})$$

$$= (E_{OH*} - E_* - E_{H_2O} + \frac{1}{2}E_{H_2}) + (E_{ZPE}(O*) - E_{ZPE}(*) - E_{ZPE}(H_2O) + \frac{1}{2}E_{ZPE}(H_2)) - T \times (S_{OOH*} - S_* - S_{H_2O} + \frac{1}{2}S_{H_2}) \quad (3)$$

$$\Delta G_{O*} = G_{O*} - G_* - (G_{H_2O} - G_{H_2})$$

$$= (E_{O*} - E_* - E_{H_2O} + E_{H_2}) + (E_{ZPE}(O*) - E_{ZPE}(*) - E_{ZPE}(H_2O) + E_{ZPE}(H_2)) - T \times (S_{OOH*} - S_* - S_{H_2O} + S_{H_2}) \quad (4)$$

$$\Delta G_{OOH*} = G_{OOH*} - G_* - (2G_{H_2O} - \frac{3}{2}G_{H_2})$$

$$= (E_{OOH*} - E_* - 2\,E_{H_2O} + \frac{3}{2}E_{H_2}) + (E_{ZPE}(OOH*) - E_{ZPE}(*) - 2E_{ZPE}(H_2O) + \frac{3}{2}E_{ZPE}(H_2)) - T \times (S_{OOH*} - S_* - 2\,S_{H_2O} + \frac{3}{2}S_{H_2}) \quad (5)$$

$$\Delta G_{H*} = G_{H*} - G_* - \frac{1}{2}G_{H_2}$$

$$= (E_{H*} - E_* - \frac{1}{2}E_{H_2}) + (E_{ZPE}(H*) - E_{ZPE}(*) - \frac{1}{2}E_{ZPE}(H_2)) - T \times (S_{H*} - S_* - \frac{1}{2}S_{H_2}) \quad (6)$$

The reaction free energy (ΔG) of the elementary steps in OER and HER was calculated as:

$$\Delta G = \Delta E_{DFT} + \Delta E_{ZPE} - T\Delta S + \Delta G_U + \Delta G_{pH} \quad (7)$$

where ΔE_{DFT} is the difference of total energy, ΔE_{ZPE} and ΔS are the differences in the zero-point energy and the change of entropy, T is 298.15 K, $\Delta G_U = -eU$ and $\Delta G_{pH} = \mathrm{pH} \times \kappa_B \mathrm{Tln10}$ are the contributions from the electrode potential (U) and pH value (κ_B is the Boltzmann constant), respectively.[2,3] Since O_2 in the triplet ground state is notoriously poorly described by DFT computations, the free energy of O_2 was derived as:

$$G_{O_2}(g) = 2\,G_{H_2O}(l) - 2\,G_{H_2}(g) + 4.92\ \mathrm{eV} \quad (8)$$

The reaction free energy of (1)-(4) for OER (at U = 0 V vs. RHE) can be calculated using the following equations:

$$\Delta G_1 = \Delta G_{OH*} \quad (9)$$

$$\Delta G_2 = \Delta G_{O*} - \Delta G_{OH*} \quad (10)$$

$$\Delta G_3 = \Delta G_{OOH*} - \Delta G_{O*} \quad (11)$$

$$\Delta G_4 = 4.92\ \mathrm{eV} - \Delta G_{OOH*} \quad (12)$$

The theoretical overpotential η_{OER} was

adopted to determine the OER activity, which was obtained based on the reaction free energies of the four elemental steps as:

$$\eta_{OER} = \max\{\Delta G_1, \Delta G_2, \Delta G_3, \Delta G_4\}/e - 1.23 \text{ V} \quad (13)$$

The reaction free energy of (5)-(6) for the HER (at $U = 0$ V vs. RHE) can be calculated using the following equations:

$$\Delta G_5 = \Delta G_{H*} \quad (14)$$

$$\Delta G_6 = -\Delta G_{H*} \quad (15)$$

For HER, the theoretical exchange current i_0 was described based on the Nørskov's assumption:[4]

$$i_0 = -e\rho k_0 \frac{1}{1 + \exp\left(\left|\Delta G_{H*}\right|/k_B T\right)} \quad (16)$$

where e is the elementary charge, ρ is the surface density of active sites which is assumed to be comparable with that of Pt(111) and the rate constant k_0 includes all effect relating to the reorganization of the solvent during the proton transfer to the surface which is assumed to be independent of the metal atom and taken as 200 s^{-1} $site^{-1}$. The obtained theoretical i_0 on Pt(111) is 4.69×10^{-4} A cm^{-2}, agreeing with the experimental value (4.5×10^{-4} A cm^{-2}).[4,5]

To evaluate the bonding strength between the main-group metal atom and the blue-P substrate, the binding energy E_b is calculated as:

$$E_b = E_{M\text{-}BP} - E_{BP} - E_M \quad (17)$$

where E_{BP} and E_M are the energy of blue-P substrate (single P vacancy) and isolated one main-group metal atom calculated by DFT, respectively. Also, to compare the bonding strength of main-group metal atom in M-BPs and in bulk metal, the cohesive energies in bulk metal (E_{coh}) are also calculated:

$$E_{coh} = \mu_{M\,(bulk)} - E_M \quad (18)$$

where $\mu_{M\,(bulk)}$ is the calculated chemical potential of main-group metal atom from the most stable bulk crystal by DFT.

Computation of the potential-dependent activation barriers

A method developed by Janik et al. was employed to determine the potential-dependent activation barriers of proton-electron transfer involved in the elementary reactions for the OER.[6-8] For an inner-sphere electrocatalytic reaction involving a proton-electron transfer, the transition state for the electrochemical reaction ($AH^* \rightarrow A^* + H^+_{(aq)} + e^-$) can be approximated to be equivalent to that of an analogous non-electrochemical reaction ($AH^* \rightarrow A^* + H^*$), at the equilibrium potential (U° vs. RHE) for the H* oxidative desorption to the bulk electrolyte ($A^* + H^* \rightarrow A^* + H^+_{(aq)} + e^-$).

Therefore, the potential-dependent activation barrier ($G^{ACT}(U)$) for the elementary electrochemical reaction can be obtained by extrapolating the activation energy ($G^{ACT}(U°)$) for the non-electrochemical dehydrogenation reaction using Bulter-Volmer theory:

$$G^{ACT}(U) = G^{ACT}(U°) - F\beta(U - U°) \quad (19)$$

where U is the applied electrode potential vs. RHE; F is the Faraday's constant; β is symmetry coefficient, which is taken as 0.6 for all steps.[9]

Figures

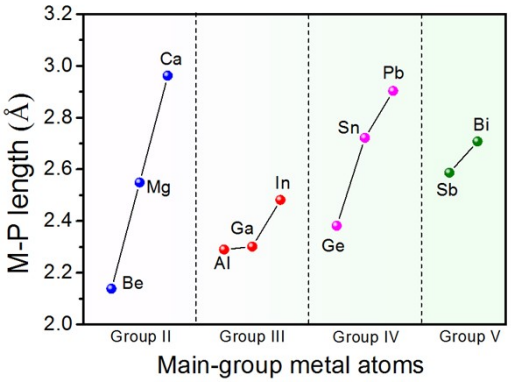

Fig. S1. The bond length of M-P in M-BPs (M = Be, Mg, Ca, Al, Ga, In, Ge, Sn, Pd, Sb, and Bi).

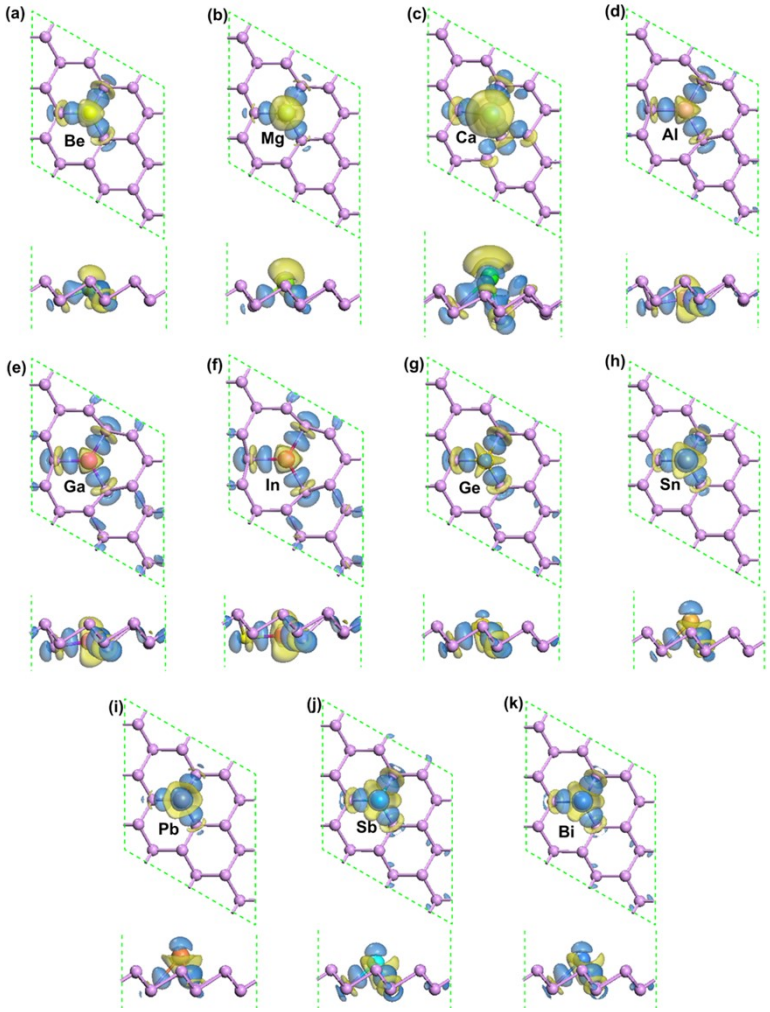

Fig. S2. The charge density difference of M-BPs where yellow and blue respectively represent the electron depletion and accumulation. The isosurface value is 0.02 e/Å^3.

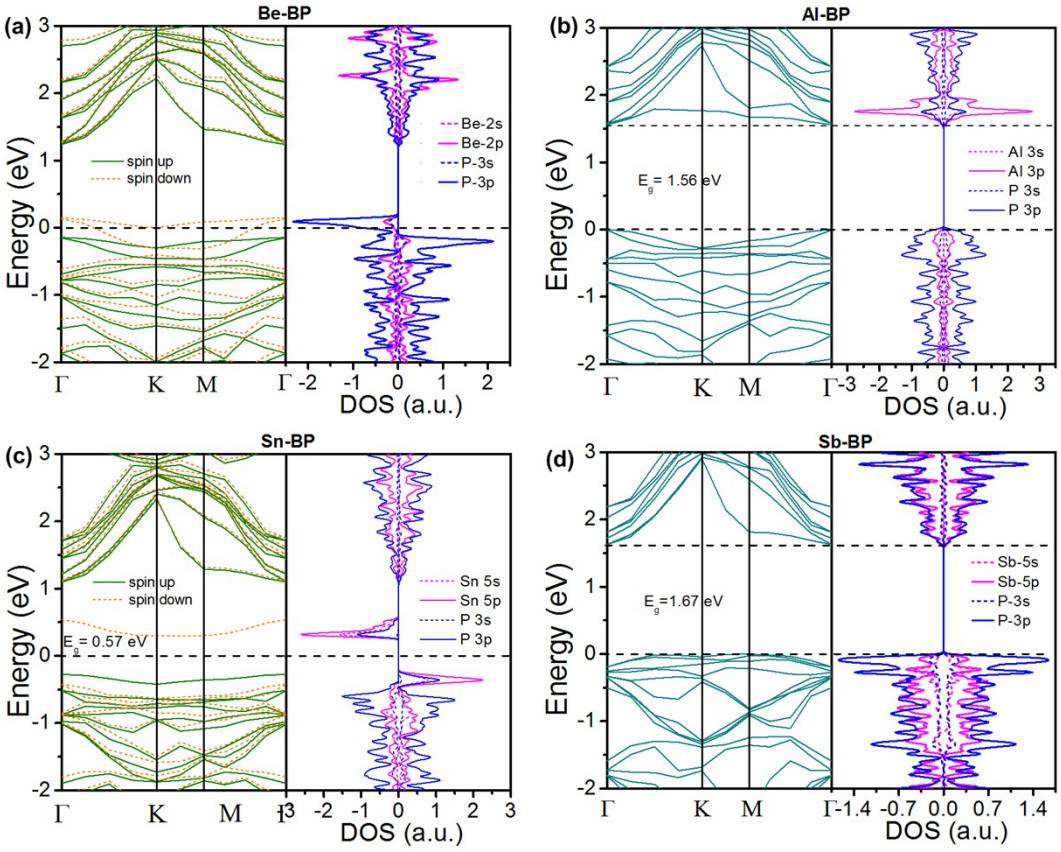

Fig. S3. Band structures and density of states (DOS) of Be, Al, Sn, and Sb-BPs.

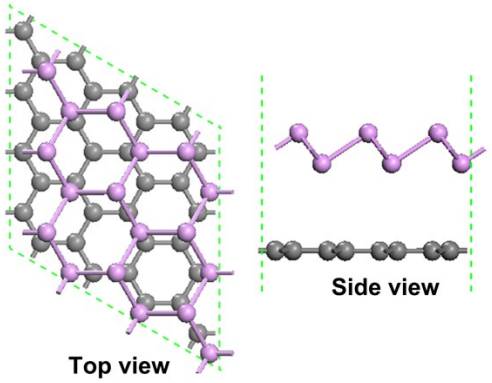

Fig. S4. Top view and side view of BP@Gra vdW heterojunction (Magenta and grey spheres represent P and C atoms, respectively).

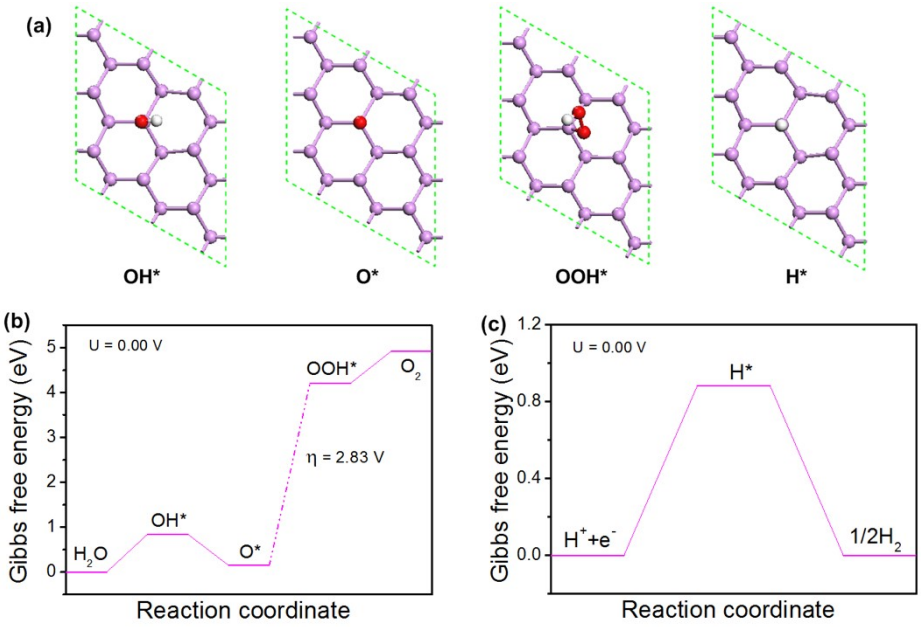

Fig. S5. (a) Optimized adsorption structures of OH*, O*, OOH*, and H* on pristine BP (Magenta, red and white spheres represent P, O, and H atoms, respectively). The reaction free energy profiles for the (b) OER and (c) HER on pristine BP at U = 0 V vs. RHE.

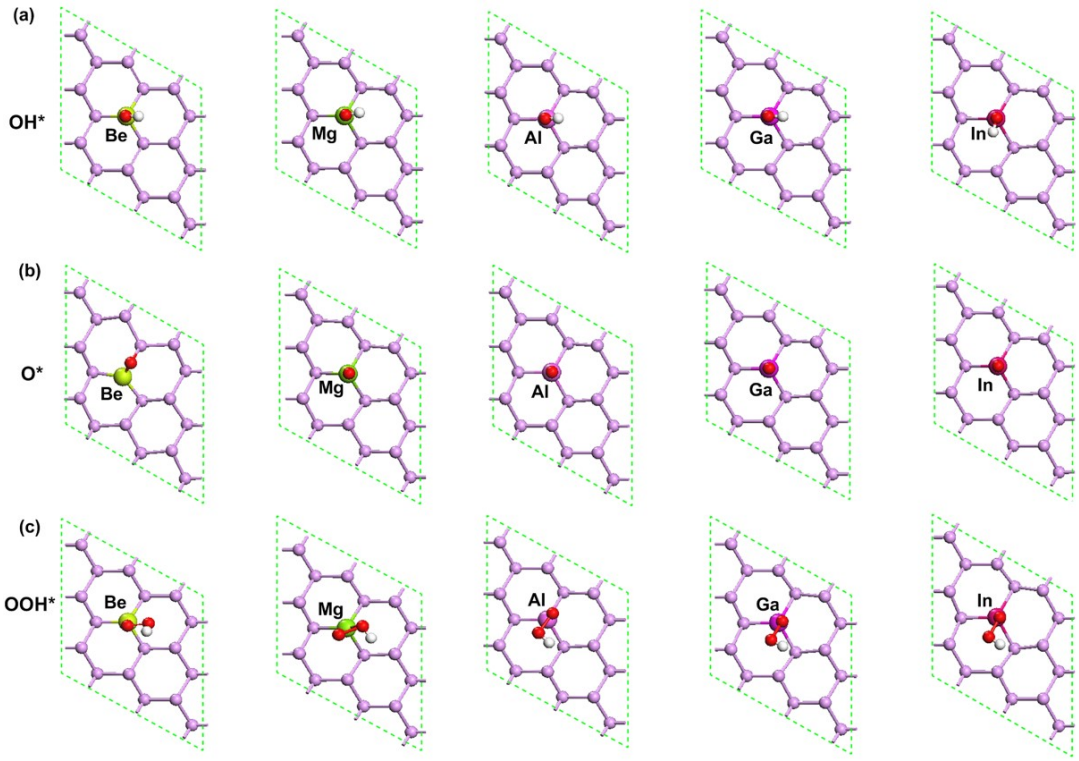

Fig. S6. Optimized adsorption structures of (a) OH*, (b) O*, and (c) OOH* on Be, Mg, Al, Ga, and In-BPs.

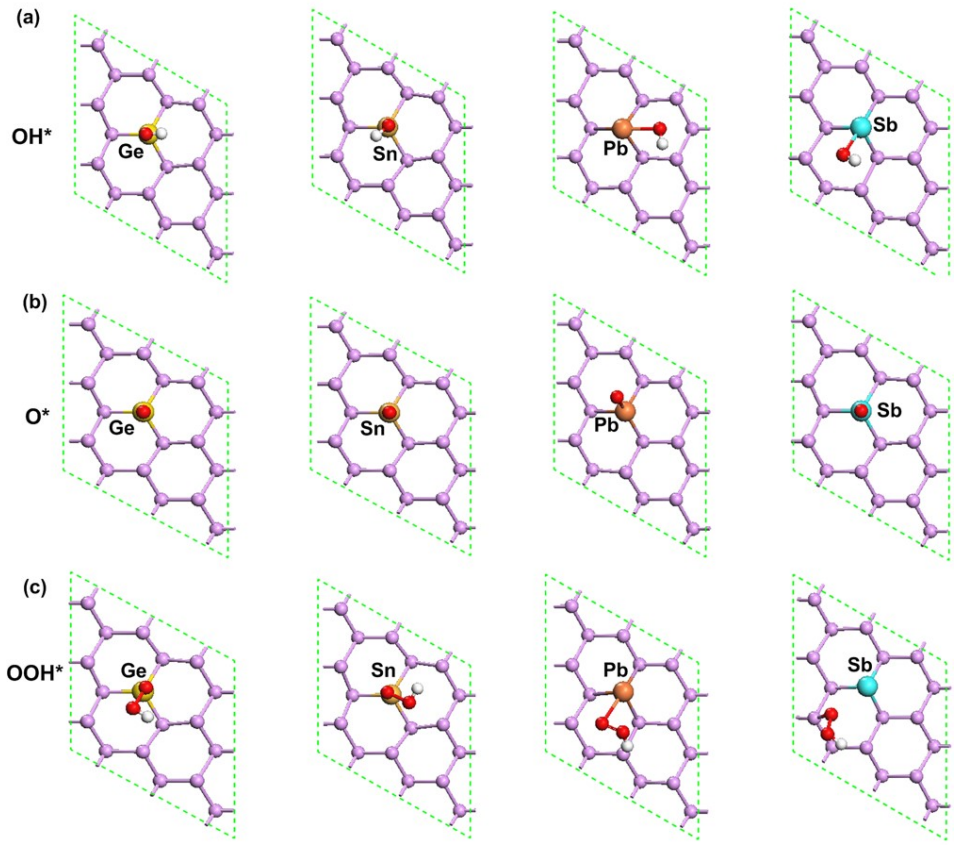

Fig. S7. Optimized adsorption structures of (a) OH*, (b) O*, and (c) OOH* on Ge, Sn, Pb, and Sb-BPs.

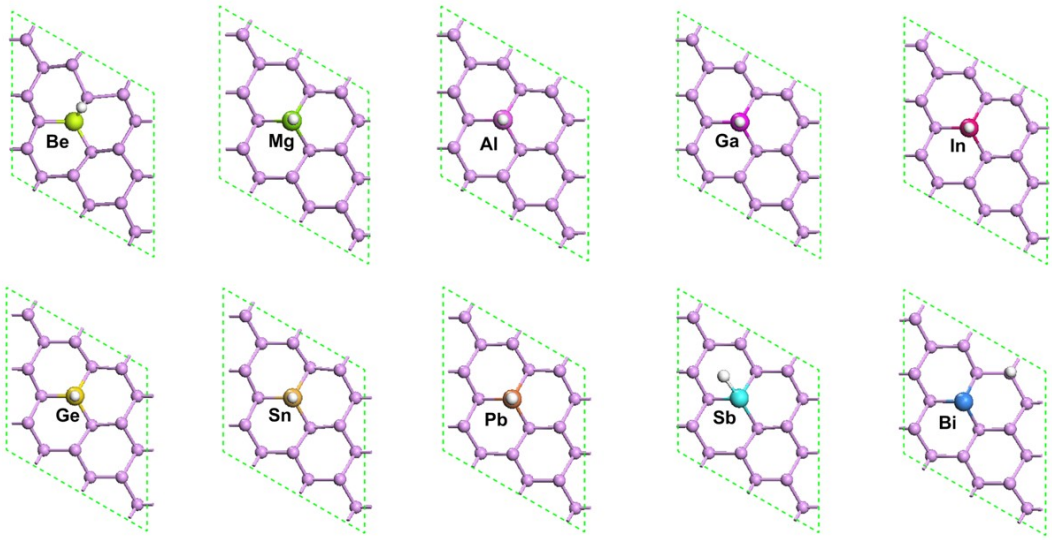

Fig. S8. Optimized adsorption structures of H* on M-BPs.

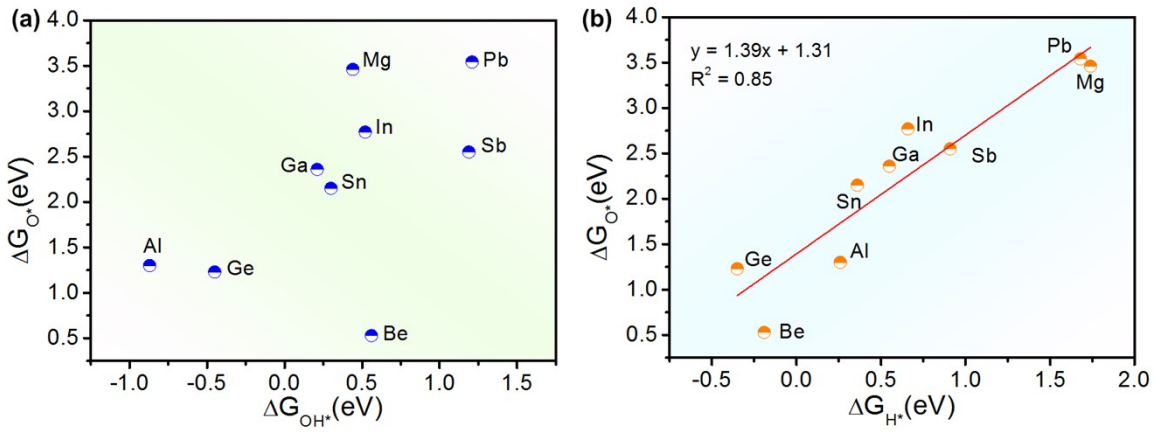

Fig. S9. ΔG_{O*} as a function of (a) ΔG_{OH*} and (b) ΔG_{H*} on M-BPs.

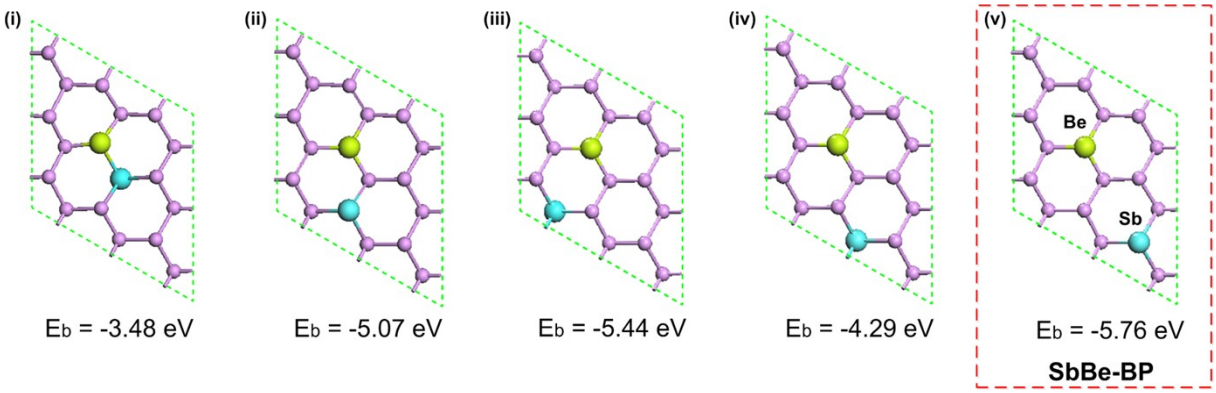

Fig. S10. Five possible structures of Sb, Be co-doped BP monolayer.

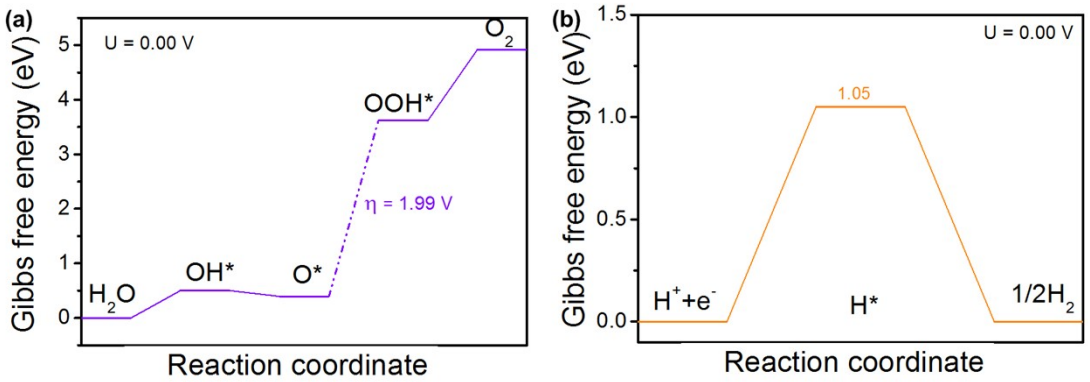

Fig. S11. (a) The reaction free energy profile for the OER on Be atom of SbBe-BP at U = 0 V vs. RHE. (b) The reaction free energy profile for the HER on Sb atom of SbBe-BP at U = 0 V vs. RHE.

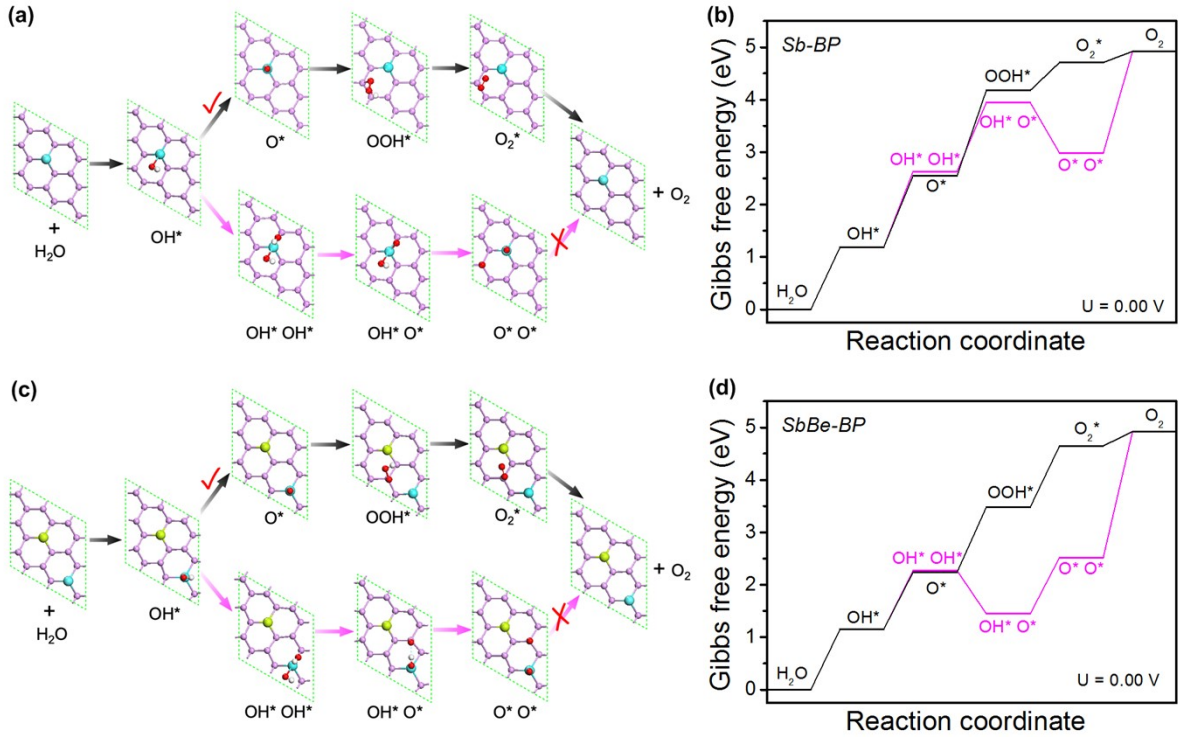

Fig. S12. The two possible OER pathways on (a) Sb-BP and (c) SbBe-BP, which include a water nucleophilic attack (WNA) mechanism via the formation of OOH* and an oxo-oxo coupling (OOC) mechanism, and (b,d) their corresponding reaction free energy profiles. (Blue, green, pink, red, and white spheres represent Sb, Be, P, O, and H atoms, respectively).

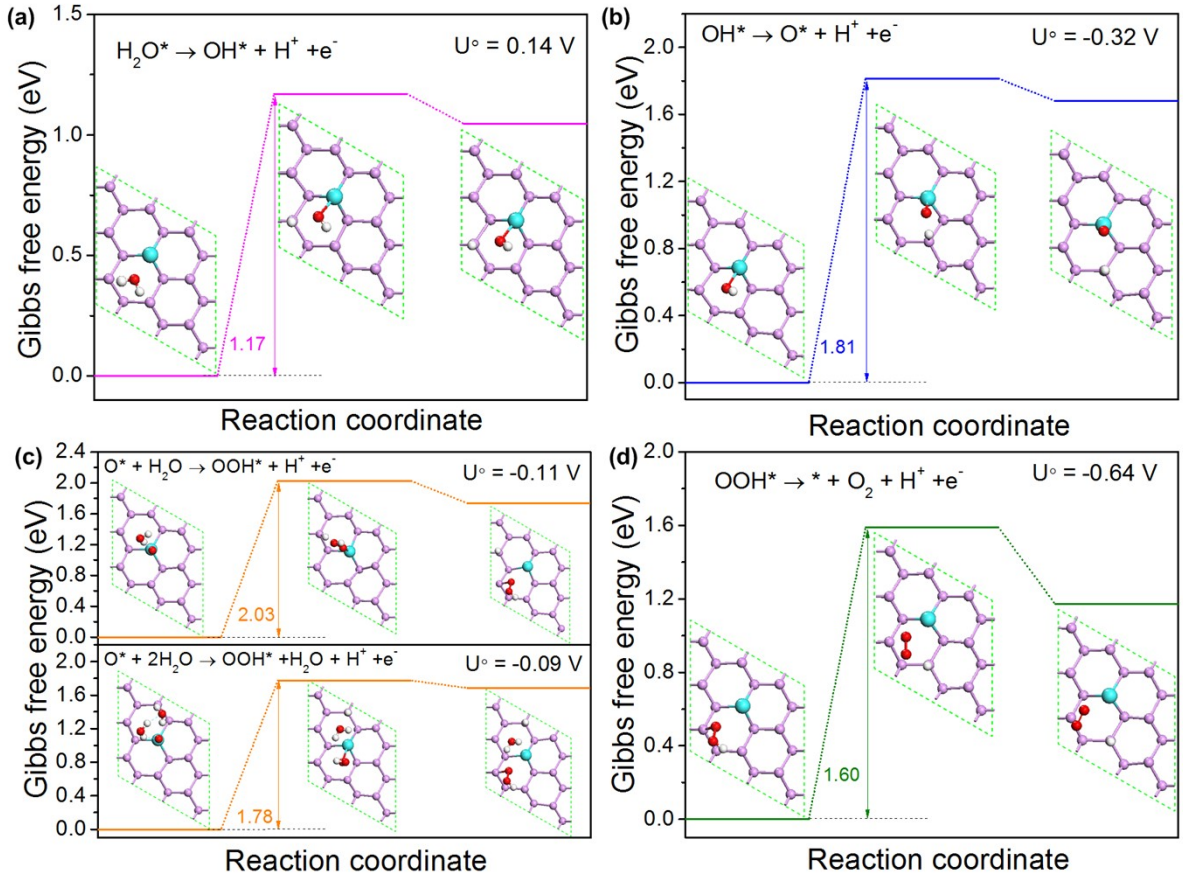

Fig. S13. The activation barriers ($G^{ACT}(U°)$) at the equilibrium potentials (U° vs. RHE) for the four elementary electrochemical steps involved in the OER on Sb-BP. There are three states from left to right, corresponding to initial, transition, and final state. (Blue, pink, red, and white spheres represent Sb, P, O, and H atoms, respectively).

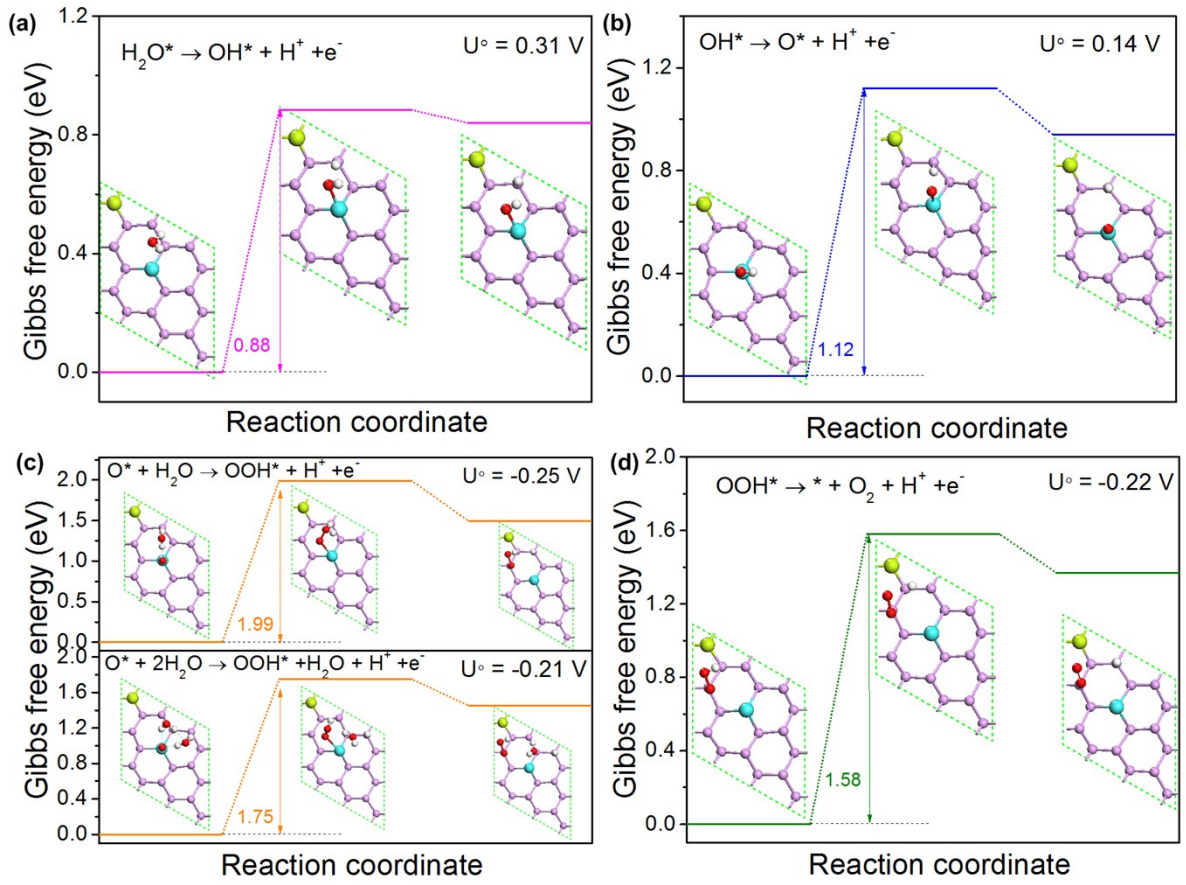

Fig. S14. The activation barriers ($G^{ACT}(U°)$) at the equilibrium potentials (U° vs. RHE) for the four elementary electrochemical steps involved in the OER on SbBe-BP. There are three states from left to right, corresponding to initial, transition, and final state. (Blue, green, pink, red, and white spheres represent Sb, Be, P, O, and H atoms, respectively).

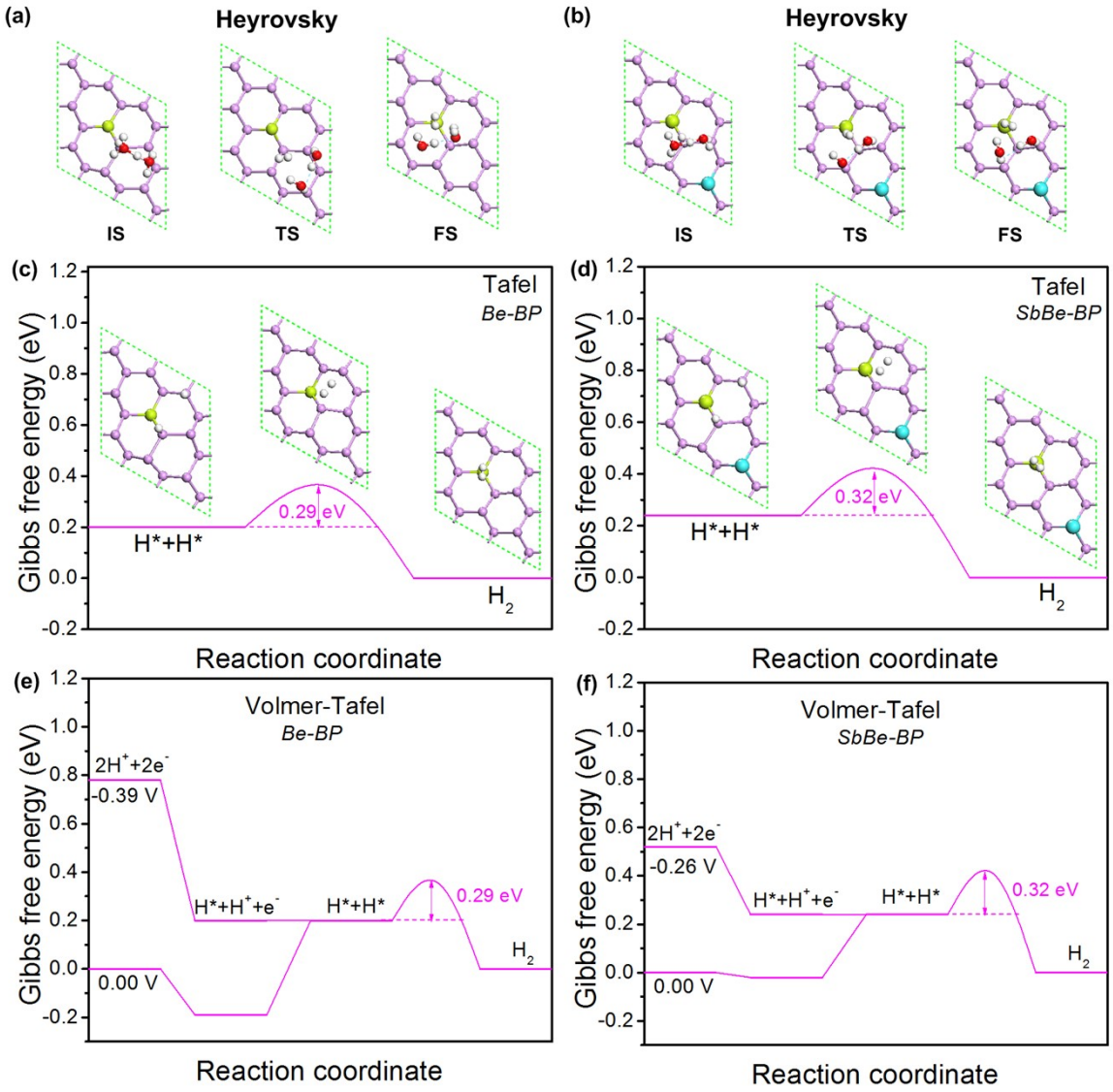

Fig. S15. The optimized structures of initial state (IS), transition state (TS) and final state (FS) of the Heyrovsky reaction on (a) Be-BP and (b) SbBe-BP. The reaction free energy profiles of the Tafel reaction including the activation barriers on (c) Be-BP and (d) SbBe-BP, and the optimized structures of IS, TS and FS are shown in the inset. (Blue, green, pink, red, and white spheres represent Sb, Be, P, O, and H atoms, respectively). The reaction free energy profiles of the HER for the Volmer-Tafel route on (e) Be-BP and (f) SbBe-BP at different electrode potentials.

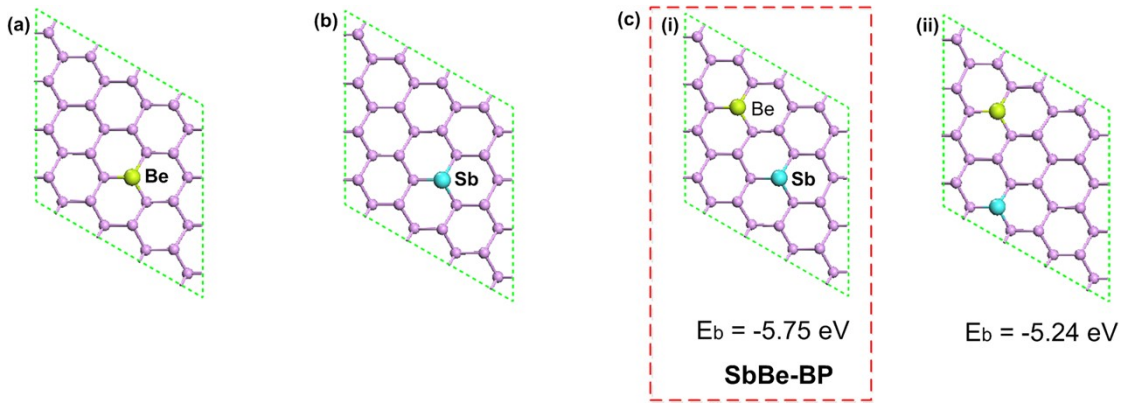

Fig. S16. Optimized structures of the 4×4 supercell samples of (a) Be-BP, (b) Sb-BP, and (c) SbBe-BP.

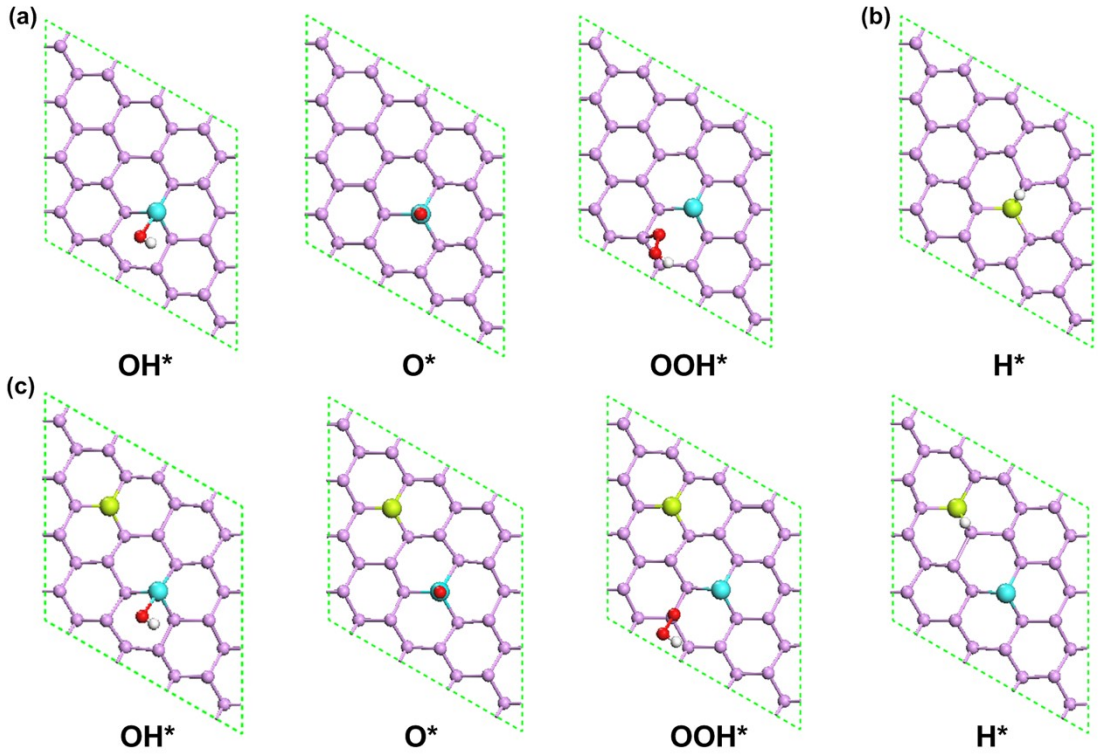

Fig. S17. (a) Optimized adsorption structures of OH*, O*, and OOH* on the 4×4 supercell Sb-BP. (b) Optimized adsorption structure of H* on the 4×4 supercell Be-BP. (c) Optimized adsorption structures of OH*, O*, OOH*, and H* on the 4×4 supercell SbBe-BP. (Blue, green, pink, red, and white spheres represent Sb, Be, P, O, and H atoms, respectively).

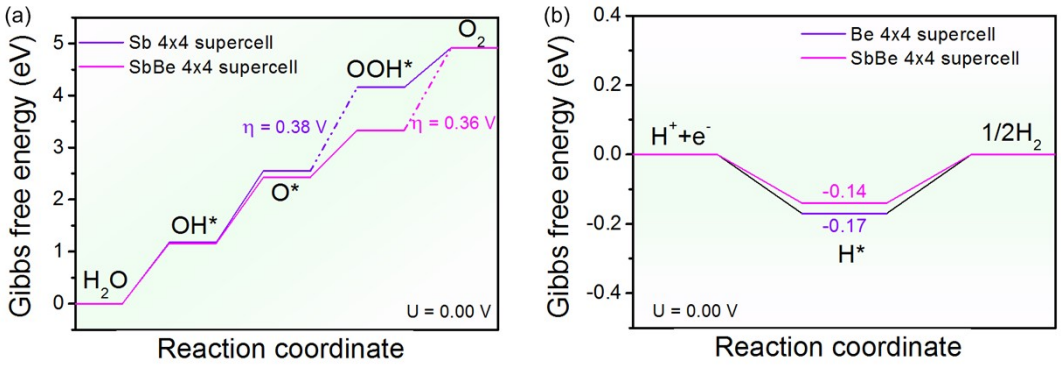

Fig. S18. (a) The reaction free energy profiles for (a) the OER on the 4×4 supercell Sb-BP and SbBe-BP and (b) the HER on the 4×4 supercell Be-BP and SbBe-BP at U = 0 V vs. RHE.

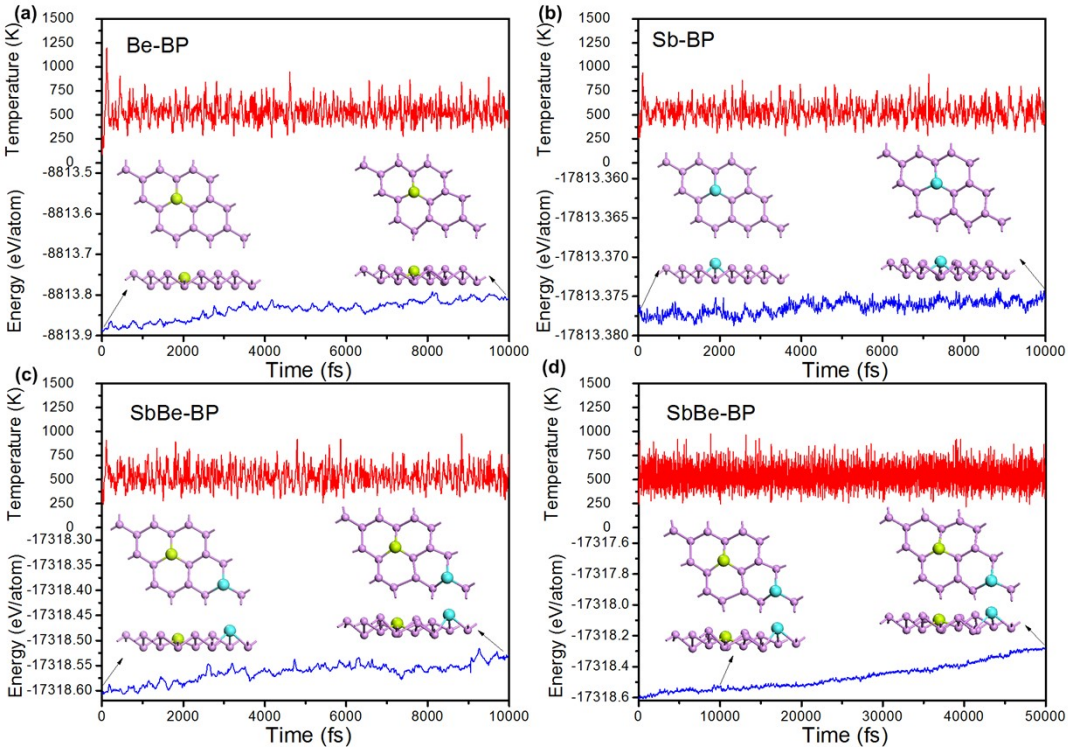

Fig. S19. Evolution of the total energy per atom and the temperature within 10 ps AIMD simulation at 500 K for (a) Sb-BP, (b) Be-BP and (c) SbBe-BP. The inset diagrams show the atomic structure at start and end of the AIMD simulation. (d) Evolution of the total energy per atom and the temperature within 50 ps AIMD simulation at 500 K for SbBe-BP. The inset diagrams show that the atomic structure of SbBe-BP remains impeccably unchanged throughout the 500K AIMD simulation, spanning from 10 ps to 50 ps. (Blue, green, and pink spheres represent Sb, Be, and P atoms, respectively).

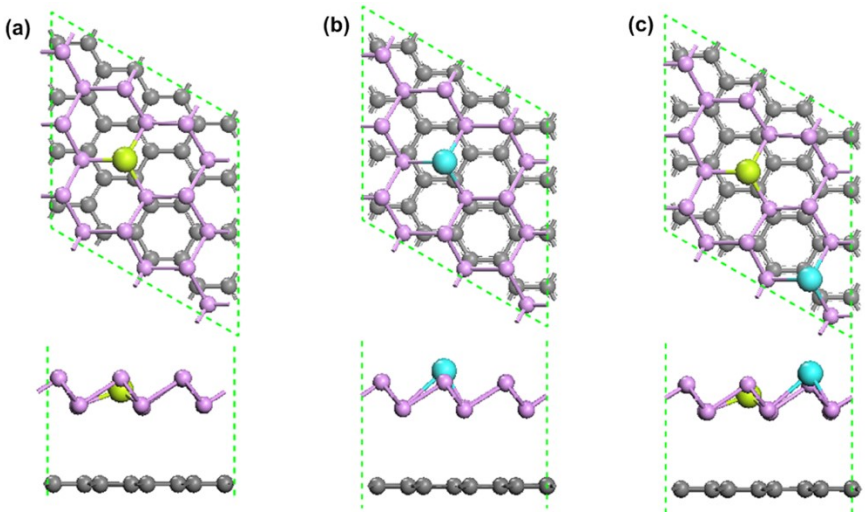

Fig. S20. Optimized structures of (a) Be-BP@Gra, (b) Sb-BP@Gra, and (c) SbBe-BP@Gra (Blue, green, pink, and grey spheres represent Sb, Be, P, and C atoms, respectively).

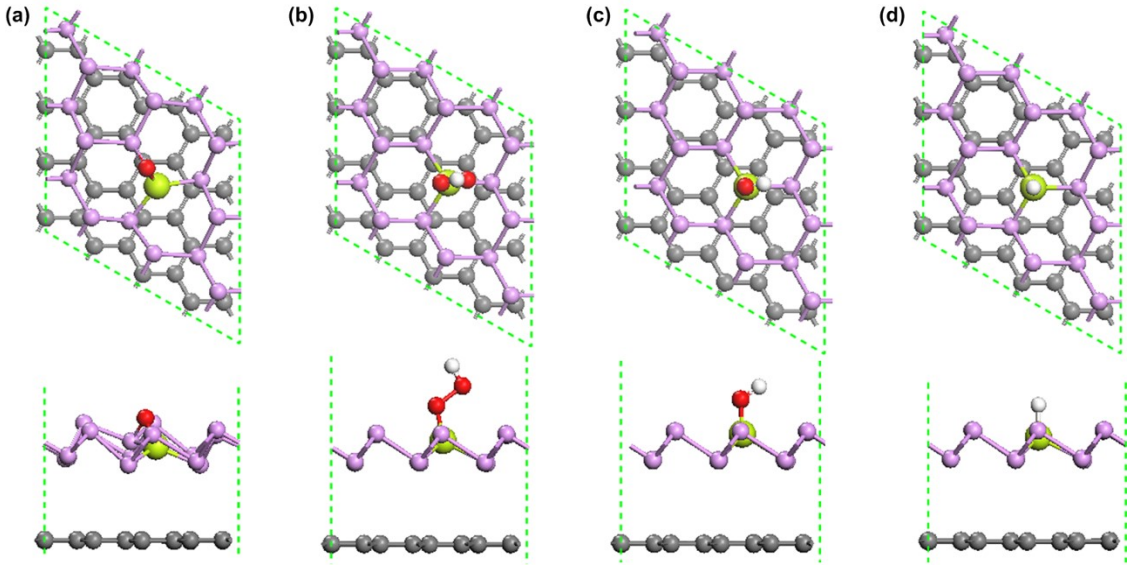

Fig. S21. Optimized structures of adsorbates ((a) O*, (b) OOH*, (c) OH*, and (d) H*) on Be atom of Be-BP@Gra (Green, pink, grey, red, and white spheres represent Be, P, C, O, and H atoms, respectively).

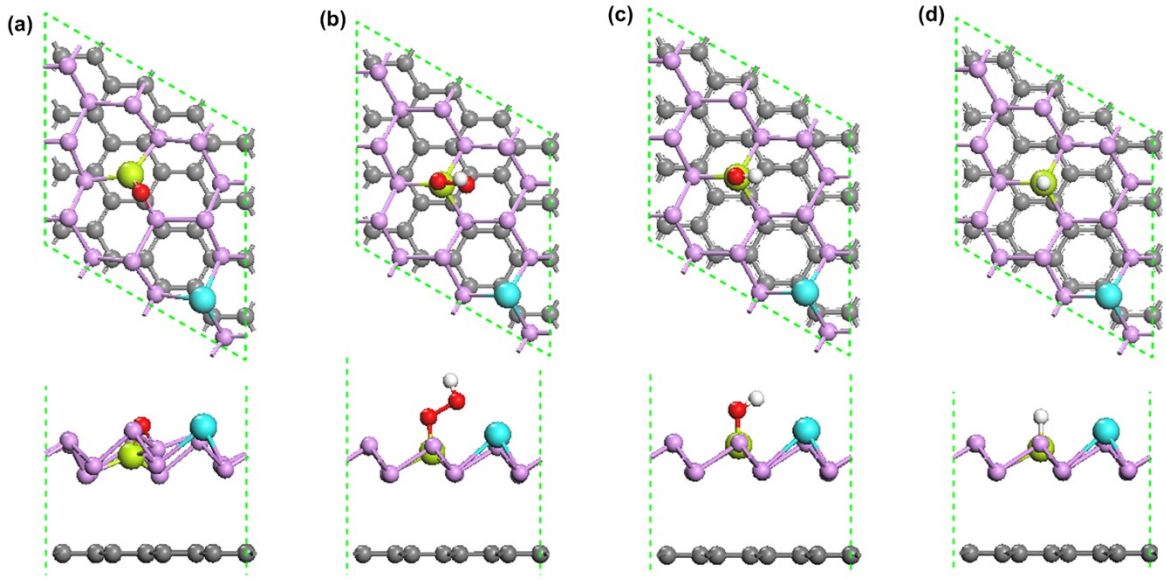

Fig. S22. Optimized structures of adsorbates ((a) O*, (b) OOH*, (c) OH*, and (d) H*) on Be atom of SbBe-BP@Gra (Blue, green, pink, grey, red, and white spheres represent Sb, Be, P, C, O, and H atoms, respectively).

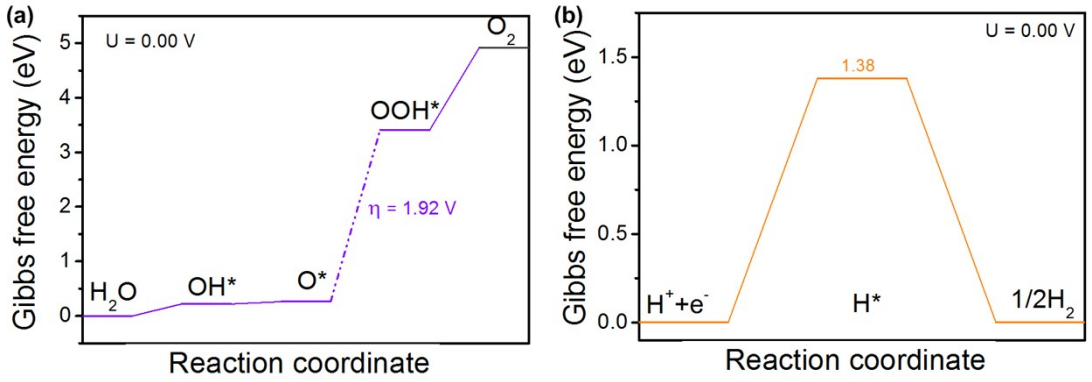

Fig. S23. (a) The reaction free energy profile for the OER on Be atom of SbBe-BP@Gra at U = 0 V vs. RHE. (b) The reaction free energy profile for the HER on Sb atom of SbBe-BP@Gra at U = 0 V vs. RHE.

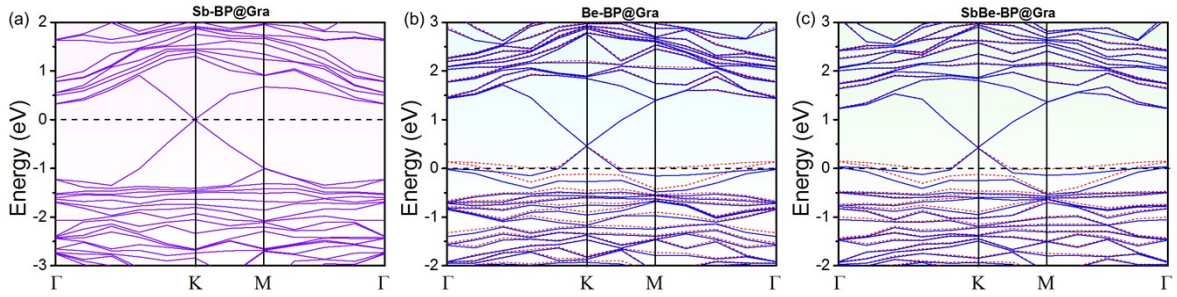

Fig. S24. The band structures of (a) Sb-BP@Gra, (b)Be-BP@Gra, and (c)SbBe-BP@Gra.

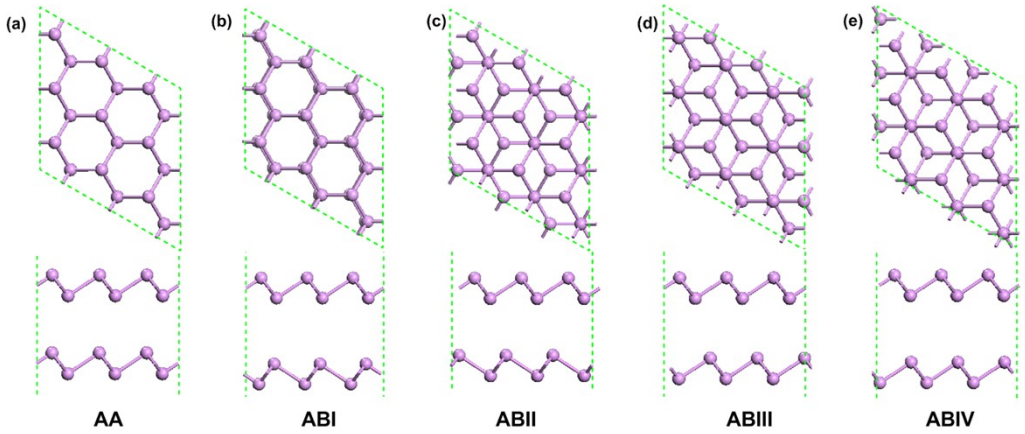

Fig. S25. Optimized structures of bilayer BP with different stacking modes.

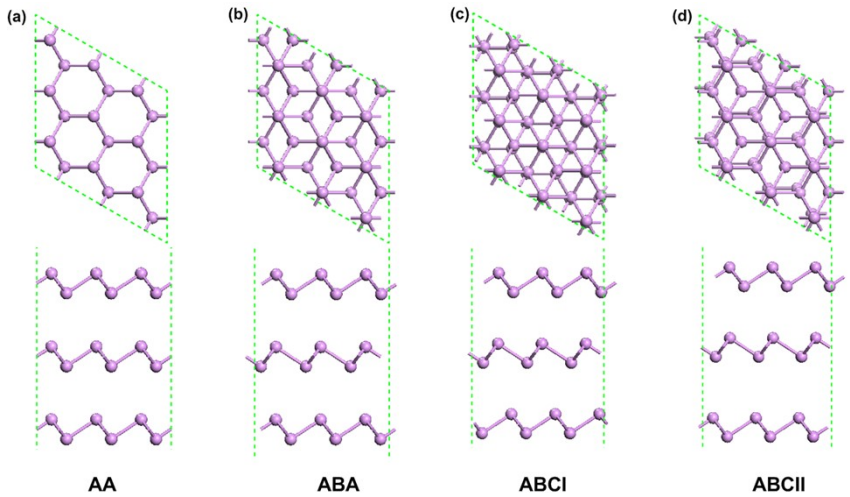

Fig. S26. Optimized structures of multi-layer BP with different stacking modes.

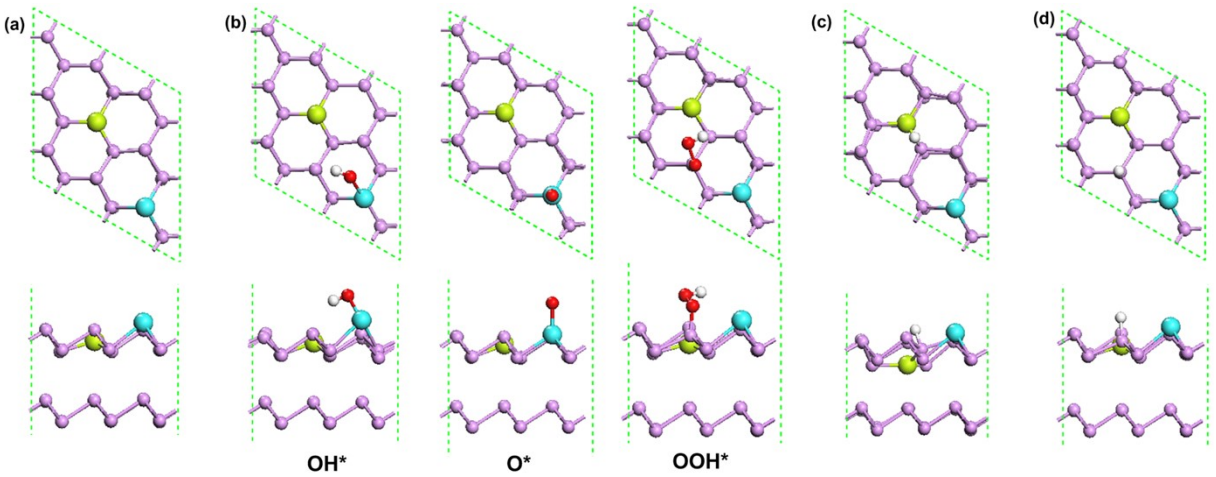

Fig. S27. (a) Optimized structure of SbBe-AA BP. (b) Optimized adsorption structures of OH*, O*, and OOH* on SbBe-AA BP. Optimized adsorption structures of H* on the (c) α P and (d) β P of Be atom in SbBe-AA BP (Blue, green, pink, red, and white spheres represent Sb, Be, P, O, and H atoms, respectively).

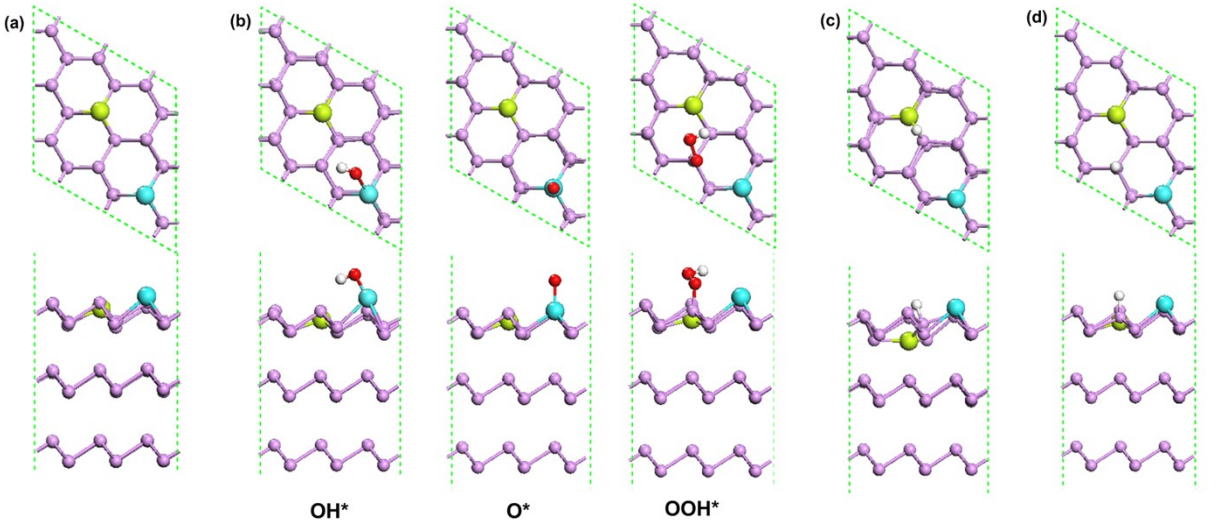

Fig. S28. (a) Optimized structure of SbBe-AAA BP. (b) Optimized adsorption structures of OH*, O*, and OOH* on SbBe-AAA BP. Optimized adsorption structures of H* on the (c) α P and (d) β P of Be atom in SbBe-AAA BP (Blue, green, pink, red, and white spheres represent Sb, Be, P, O, and H atoms, respectively).

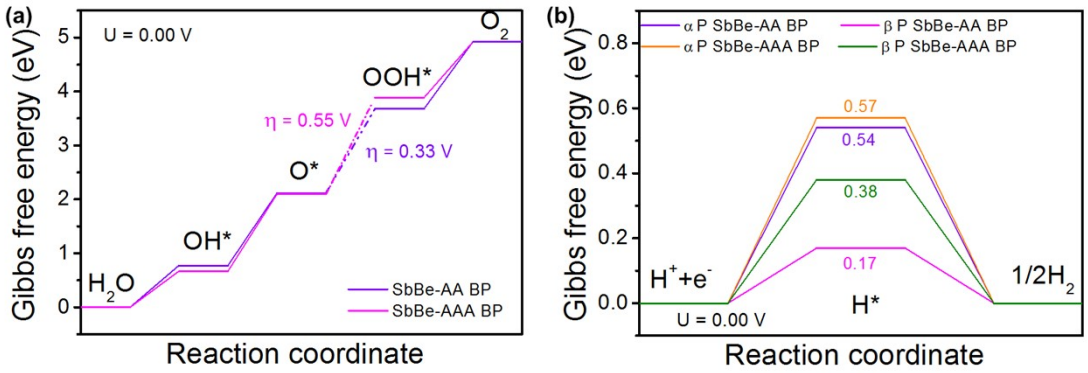

Fig. S29. (a) The reaction free energy profiles for the OER on SbBe-AA BP and SbBe-AAA BP at U = 0 V vs. RHE. (b) The reaction free energy profiles for the HER on the α P and β P of Be atom in SbBe-AA BP and SbBe-AAA BP at U = 0 V vs. RHE.

Tables

Table S1. Lattice constants (a × b) of M-BPs (c = 25 Å, α = β = 90°, γ = 120°). All results are in unit of $Å^2$.

Be	Mg	Ca	Al
10.02 × 10.02	10.00 × 10.00	9.92 × 9.92	9.92 × 9.92
Ga	In	Ge	Sn
10.05 × 10.05	10.18 × 10.18	10.03 × 10.03	10.00 × 10.00
Pb	Sb	Bi	
9.98 × 9.98	10.02 × 10.02	10.04 × 10.04	

Table S2. The bond length of M-P, the atomic radii (R_M) of M atom, the binding energy (E_b) between M atom and its adjacent P atoms in M-BPs, the cohesive energy (E_{coh}) of M atom in bulk main-group metal, the Hirshfeld charge (Q_M) of M atom of M-BPs, and the first ionization energies (I_1) of M atom.

M-BP	M-P (Å)	R_M (Å)	E_b (eV)	E_{coh} (eV)	Q_M (e)	I_1 (10^2 kJ mol^{-1})
Be	2.14	0.89	-6.20	-3.92	0.26	9.00
Mg	2.55	1.36	-3.79	-1.54	0.57	7.38
Ca	2.96	1.74	-5.10	-2.01	0.71	5.90
Al	2.29	1.18	-5.35	-3.46	0.26	5.78
Ga	2.30	1.26	-4.76	-2.73	0.24	5.79
In	2.48	1.42	-4.24	-2.38	0.36	5.58
Ge	2.38	1.22	-4.98	-3.63	0.08	7.62
Sn	2.72	1.41	-4.16	-3.03	0.23	7.09
Pb	2.90	1.54	-3.78	-2.60	0.39	7.16
Sb	2.59	1.43	-4.66	-2.81	0.24	8.31
Bi	2.71	1.52	-4.11	-2.47	0.35	7.03

Table S3. The interlayer binding energy (E_{IB}), equilibrium interlayer distance (D_{eq}) and lattice constant (a × b) of vdW heterojunctions.

vdW heterojunctions	E_{IB} (eV)	D_{eq} (Å)	a × b (Å^2)
BP@Gra	-1.59	3.55	9.86 × 9.86
Be-BP@Gra	-1.72	3.51	9.86 × 9.86
Sb-BP@Gra	-1.58	3.51	9.86 × 9.86
SbBe-BP@Gra	-1.64	3.55	9.86 × 9.86

Table S4. Values of ΔG_{OH*}, ΔG_{O*}, ΔG_{OOH*}, and ΔG_{H*} on M-BPs.

M-BP	ΔG_{OH*} (eV)	ΔG_{O*} (eV)	ΔG_{OOH*} (eV)	ΔG_{H*} (eV)
Be	0.56	0.53	3.66	-0.19
Mg	0.44	3.46	3.59	1.74
Al	-0.87	1.30	2.47	0.26
Ga	0.21	2.36	3.37	0.55
In	0.52	2.77	3.60	0.66
Ge	-0.45	1.23	2.79	-0.35
Sn	0.30	2.15	3.53	0.36
Pb	1.19	2.55	4.18	0.91
Sb	1.21	3.54	4.12	1.68
Bi	--	--	--	0.85

Table S5. Reaction free energy of every CPET step and the value of overpotential η for OER on M-BPs.

M-BP	ΔG_1 (eV)	ΔG_2 (eV)	ΔG_3 (eV)	ΔG_4 (eV)	η_{OER} (V)
Be	0.56	-0.03	3.13	1.26	1.90
Mg	0.44	3.02	0.13	1.33	1.79
Al	-0.87	2.17	1.17	2.45	1.22
Ga	0.21	2.15	1.01	1.55	0.92
In	0.52	2.25	0.83	1.32	1.02
Ge	-0.45	1.68	1.56	2.13	0.90
Sn	0.30	1.85	1.38	1.39	0.62
Pb	1.21	2.33	0.58	0.80	1.10
Sb	1.19	1.36	1.63	0.74	0.40

Table S6. The interlayer binding energy (E_{IB}) and the height of Be (h_{Be}) in bare and intermediate-adsorbed Be-BP@Gra, as well as the variation of E_{IB} (ΔE_{IB}) induced by intermediates.

Be-BP@Gra	E_{IB} (eV)	h_{Be} (Å)	ΔE_{IB} (eV)
Bare	-1.72	0.75	0.00
H*-α P	-1.29	0.37	0.43
H*-β P	-1.61	0.87	0.11
H*- Be	-1.89	0.99	-0.17
O*-Be	-1.81	0.78	-0.09
OOH*-Be	-1.82	1.06	-0.10
OH*-Be	-1.84	1.13	-0.12

Table S7. The interlayer binding energy (E_{IB}) and the height of Be (h_{Be}) in bare and intermediate-adsorbed SbBe-BP@Gra, as well as the variation of E_{IB} (ΔE_{IB}) induced by intermediates.

SbBe-BP@Gra	E_{IB} (eV)	h_{Be} (Å)	ΔE_{IB} (eV)
Bare	-1.64	0.75	0.00
H*-α P	-1.29	0.30	0.35
H*-β P	-1.55	0.71	0.09
H*- Be	-1.83	1.02	-0.19
O*-Be	-1.73	0.83	-0.09
OOH*-Be	-1.76	1.01	-0.12
OH*-Be	-1.78	1.15	-0.14

Table S8. The interlayer binding energy (E_{IB}), equilibrium interlayer distance (D_{eq}) and lattice constant (a × b) of bilayer BP with different stacking modes (c = 27 Å, α = β = 90°, γ = 120°).

stacking modes	E_{IB} (eV)	D_{eq} (Å)	a × b (Å^2)
AA	-1.09	3.43	9.87 × 9.87
ABI	-0.74	4.08	9.88 × 9.88
ABII	-1.07	3.44	9.90 × 9.90
ABIII	-0.98	3.62	9.89 × 9.89
ABIV	-0.76	4.06	9.88 × 9.88

Table S9. The average interlayer binding energy (E_{IB}), average equilibrium interlayer distance (D_{eq}) and lattice constant (a × b) of multi-layer BP with different stacking modes (c = 30 Å, α = β = 90°, γ = 120°).

stacking modes	E_{IB} (eV)	D_{eq} (Å)	a × b (Å^2)
AAA	-1.14	3.38	9.87 × 9.87
ABA	-1.12	3.40	9.90 × 9.90
ABCI	-1.12	3.42	9.90 × 9.90
ABCII	-0.95	3.75	9.90 × 9.90

References

1 J. K. Nørskov, A. Logadottir and L. Lindqvist, *J. Phys. Chem. B*, 2004, **108**, 17886-17892.

2 L. Yu, X. Pan, X. Cao, P. Hu and X. Bao, *J. Catal.*, 2011, **282**, 183-190.

3 H. Xu, D. Cheng, D. Cao and X. C. Zeng, *Nat. Catal.*, 2018, **1**, 339.

4 J. K. Nørskov, T. Bligaard, A. Logadottir, J. R. Kitchin, J. G. Chen, S. Pandelov and U. Stimming, *J. Electrochem. Soc.*, 2005, **152**, J23.

5 E. Skúlason, V. Tripković, M. E. Bjo¨rketun, S. Gudmundsdo´ttir, G. Karlberg, J. Rossmeisl, T. Bligaard, H. Jo´nsson and J. K. Nørskov, *J. Phys. Chem. C*, 2010, **114**, 18182-18197.

6 S. A. Akhade, N. J. Bernstein, M. R. Esopi, M. J. Regula and M. J. Janik, *Catal. Today*, 2017, **288**, 63-73.

7 X. Z. Chen, X. J. Zhao, Z. Z. Kong, W.-J. Ong and N. Li, *J. Mater. Chem. A*, 2018, **6**, 21941-21948.

8 J. Resasco, F. Abild-Pedersen, C. Hahn, Z. Bao, M. T. M. Koper and T. F. Jaramillo, *Nat. Catal.*, 2022, **5**, 374-381.

9 J. Zhang, H. B. Tao, M. Kuang, H. B. Yang, W. Cai, Q. Yan, Q. Mao and B Liu, *ACS Catal.*, 2020, **10**, 8597-8610.